J Mater Sci (2007) 42:2717–2723
DOI 10.1007/s10853-006-1406-8

Electrode coatings for high temperature hydrogen electrolysis

W. E. Windes · C. Smith · D. Wendt · A. Erickson · J. Walraven · P. A. Lessing

Received: 8 July 2005 / Accepted: 22 February 2006 / Published online: 9 January 2007

Abstract A discussion of fabrication techniques and performance testing of solid oxide components for use in hydrogen steam electrolysis is presented. Novel plasma spray techniques are utilized to deposit the thin ceramic oxide electrode, electrolyte, and interconnect layers on a planar intermetallic bipolar plate. Optimal porosity is achieved within the electrode microstructure through mixed feed techniques that are a combination of dry powder feed and liquid solution injection. The perovskite anode coatings formed from liquid precursor feedstock require post-deposition annealing in an oxygen-rich atmosphere to form the desired perovskite structures. Electrical conductivity measurements were measured for all electrodes and interconnect materials as a function of temperature to 1000 °C.

Introduction

The prospect of a ''Hydrogen Economy'' has generated a great deal of interest both in technical and political circles over the past few years. This new economy will rely upon hydrogen as the energy carrier for both electrical and non-electrical applications. Today, we have a centralized system of generation and distribution of hydrocarbon fuels and electricity. In order for the ''Hydrogen Economy'' to become a reality, a considerable quantity of low-cost hydrogen will need to be generated and distributed in order to meet the demands of this new energy distribution system [1, 2].

Hydrocarbon reforming (primarily steam reforming of methane) is the preferred method used to produce hydrogen for present day applications. However, hydrocarbon reforming practices are not viable for future large-scale production of hydrogen nor is it compatible with the principle behind the hydrogen economy since non-renewable resources are consumed and greenhouse gases are generated. Consequently, there is considerable interest in producing hydrogen from the splitting of water utilizing either thermochemical or electrolytic processes [3].

Hydrogen produced using heat and electricity from high temperature nuclear reactors has been proposed as a highly efficient and environmentally acceptable alternative [4] to steam reforming. In particular, the ''Next Generation Nuclear Plant (NGNP)'' program is specifically intended to combine a nuclear reactor having a very high temperature outlet temperature (in excess of 1000°C) with a high temperature hydrogen generation plant.

As the lead DOE laboratory for nuclear research, the Idaho National Laboratory (INL) has led the effort in developing nuclear hydrogen generators for the NGNP program. The INL has specifically focused upon the research and scale-up issues associated with solid oxide electrolysis cell technology for hydrogen production [5–7]. High temperature electrolysis uses solid oxide fuel cells (SOFC) in a steam electrolysis mode to generate hydrogen. By using pre-existing

Supported by the U.S. Department of Energy, Office of Nuclear Energy Science and Technology, under the DOE Idaho Operations Contract No. DE-AC07-05ID14517

W. E. Windes (✉) · C. Smith · D. Wendt · A. Erickson · J. Walraven · P. A. Lessing
Idaho National Laboratory, 2351 N. Boulevard, Idaho Falls, ID 83415-2218, USA
e-mail: william.windes@inl.gov

technology, development costs are reduced and full advantage can be taken from the high temperature efficiencies anticipated for SOFCs. Indeed, significant progress has been achieved for many of the material and design problems encountered for these high temperature systems that make them promising for hydrogen production.

Building upon previous INL solid oxide materials development experience [8, 9] electrolytic cells have been fabricated, characterized, and tested at expected operating temperatures. The INL cell is interconnect supported allowing the deposition of very thin electrode and electrolyte coatings. Optimal microstructures for both types of coatings were achieved by utilizing liquid injection plasma deposition (LIPD) techniques. In the LIPD technique, solutions containing constituent materials for either electrode or electrolyte coatings are injected into the plasma to produce a very thin, solid (or porous), and adherent coating on the supporting interconnect substrate.

Solid particle formation within the plasma occurs by gas-phase nucleation of the LIPD precursor solutions. The liquid solution is atomized into small droplets before being injected into the plasma flame. The droplets are then rapidly heated, causing the formation of extremely small solid nuclei that grow rapidly within the plasma. The size and number of particles precipitated within the plasma is dependent upon the plasma temperature, time within the plasma, concentration of the liquid precursor, and feed rate of the deposition material [10, 11]. Manipulating these key parameters allows the microstructure of the deposited material to be controlled and optimized.

The present study discusses several of the key process parameters necessary to produce optimal electrode and electrolyte coatings for the new electrolytic cells. Microstructure characterization, crystal structure, and electrical conductivity tests demonstrate that the deposited coatings are capable of maximum efficiency at operating temperatures of 1000°C.

Experiment

Electrode fabrication

For the INL design, oxide coatings are sequentially deposited upon a relatively thick nickel–aluminide (NiAl intermetallic composition) plate to form an interconnect-supported SOFC plate [8]. Fabrication methods, plate characteristics, and thermal properties for the intermetallic bi-polar plate have been discussed in detail elsewhere [9]. The NiAl substrate is designed to provide a thermally stable (T_m = 1638°C) and mechanically strong foundation to support the thin layers comprising the working components of the electrolysis cell (See Fig. 1). For this particular study, individual electrode coatings (i.e. cathode and anode) were plasma deposited upon small, round (25.4-mm dia. × 4-mm thick) NiAl intermetallic substrates for electrical conductivity testing.

A plasma deposition system (Metco MBN plasma gun) was used to deposit all coatings upon the NiAl substrate. Both liquid and dry powder material injection systems were used to produce electrode microstructures with maximum porosity. Dry powder feedstock from a standard fluidized powder bed feeder (Metco 4MP powder feeder) was plasma sprayed in conjunction with a custom fabricated liquid injection plasma deposition (LIPD) system (Shown in Fig. 2) to produce the porous electrode layers. Yttria-stabilized zirconia [$(ZrO_2)_{0.8}(Y_2O_3)_{0.2}$] dry powder (Praxair ZRO-299) was used for both anode and cathode layers. The dense electrolyte layer was formed using sequential LIPD and atomic layer chemical vapor deposition (ALCVD) techniques, as discussed elsewhere [12].

The LIPD technique uses an aqueous solution of nitrate salts as the precursor feedstock solution (See Table 1). A commercially available airbrush system (See Fig. 2) was used to atomize the liquid and inject the LIPD droplets into the plasma. The atomizing gas and gas carrier pressure remained fairly constant at 12 psig for all depositions. Liquid injection rates were controlled using dual-syringe pumps (Cole-Parmer 74900 series) with a feed rate ranging from 5–35 ml/min depending upon desired porosity and coating thickness. Electrode coating thickness ranged from 25–100 μm.

After each electrode deposition, the coatings were heat treated (30 min at 800°C) to decompose any remaining nitrate salts. The Nickel-YSZ layers (cathode) were heated in a flowing nitrogen atmosphere to preclude oxidation of the nickel deposit while Lanthanum–Strontium–Manganite [$(La_xSr_y)MnO_3$] anode layers were heated in air to allow the perovskite oxide structure to form from the precursor materials.

XRD (Bruker AXS D8 Advance) was utilized to determine the crystal structure and SEM (Phillips XL30 ESEM) was used for visual and elemental characterization of all deposited layers after heat treatment. High temperature electrical conductivity testing of the electrode layers was performed within a custom built apparatus, described below.

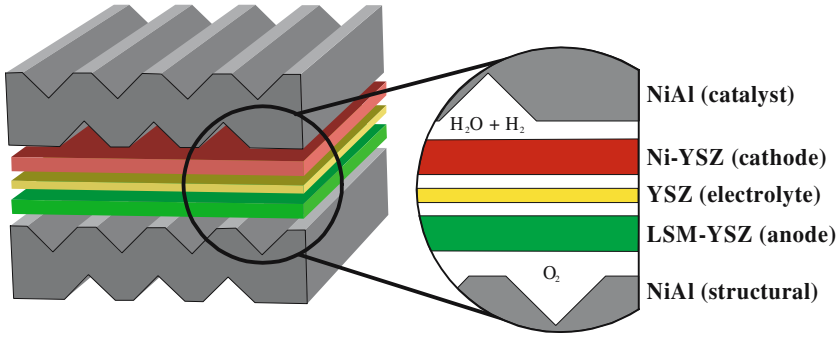

Fig. 1 Schematic diagram of SOEC structure

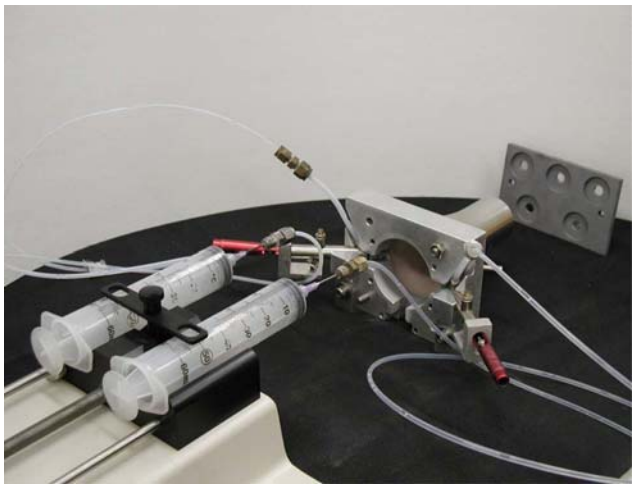

Fig. 2 LIPD equipment (mockup). Left, programmable pump with syringes; Center, air brush injectors, holder, and shrouds; Right, sample holder for multiple round substrates

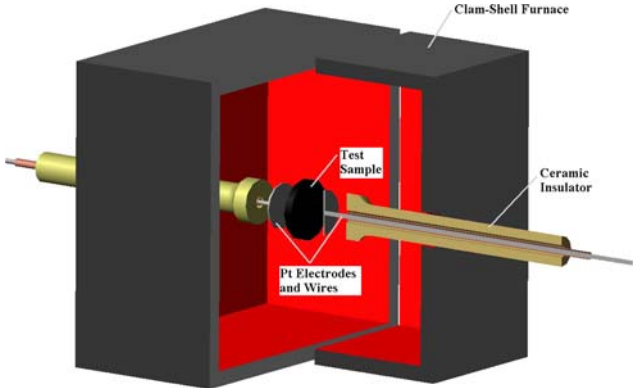

Fig. 3 Schematic of electrical conductivity apparatus

Electrical testing

A high temperature electrical test apparatus was developed for testing the deposited electrodes and intermetallic substrates (See Fig. 3). Each test sample was placed within an electrically insulating ceramic holder with platinum electrodes on both sides. Platinum wire inside of the ceramic holders connected the electrodes to the outside of a simple clam-shell furnace for probe connection. The ceramic holders were spring tightened (not shown) to insure good contact between electrodes and sample at all temperatures. Platinum paste (Engelhard, stock #A4338) was applied to both faces of the sample to enhance electrical contact over the entire test temperature range.

PC4 cell cable probes (Gamry Instruments) connected the platinum wire to a potentiostat used in conjunction with Gamry Instruments software (FrameWork "DC105") to perform electrical resistive measurements at all temperatures. The potentiostat controlled the voltage difference between the test sample electrodes (the working electrode) and an internal reference electrode allowing the current flow between the working and auxiliary electrodes to be monitored. Electrical conductivity at all temperatures was derived from the applied voltage and measured current across the faces of the samples. Normalized values, rather than individual measurements, for each sample were calculated from the sample surface area and thickness.

The electrical conductivity of each sample was tested from room temperature to 1000°C in 50 °C increments perpendicular to the plane of the coating.

Table 1 Liquid precursor feedstock solutions

Metal nitrate solutions	Molar concentration, M
LSM—(La_xSr_y)Mn oxide	
$La(NO_3)_3{\cdot}6H_2O$	0.78 M
$Sr(NO_3)_2$	0.20 M
$Mn(NO_3)_2$ xH_2O	1.40 M
Ni	
$Ni(NO_3)_2{\cdot}6H_2O$	2.6 M
YSZ—$(ZrO_2)_x(Y_2O_3)_y$	
25% ZON (zirconium oxynitrate)	2.86 M
$Y_2(CO_3)_3{\cdot}3H_2O$	0.134 M

The sample temperature was allowed to stabilize before the electrical conductivity was measured. All high temperature tests were conducted in flowing argon to minimize oxidation of the samples. Each sample was scanned at 10 mV/s voltage potential rate at a sample period of 0.1 s. This was repeated every 24 s for a total time of 144 s yielding six distinct data points at each temperature increment. The average value was calculated and recorded for each temperature increment.

Results & discussion

Electrode microstructures

Electrode coatings utilizing LSM (anode) and Ni (cathode) active constituents require considerable porosity within the microstructure to enhance gas transport efficiency and provide a larger number of triple-points (gas/electrode/electrolyte) to enhance electrochemical reduction or oxidation reactions at the electrolyte interface. The microstructures fabricated with the LIPD process were designed to provide a maximum of porosity while still maintaining some electrical conductivity within each electrode layer. Additionally, a significant volume of YSZ powder material (visually estimated to be 30–50 vol%) was added to both electrode layers to bring the coefficient of thermal expansion (CTE) of the electrodes closer to the electrolyte values.

Figure 4a and b show typical microstructures of the deposited cathode (Ni + YSZ) and anode (LSM + YSZ) electrode coatings, respectively. The bulk of the composite electrode deposit is seen to consist primarily of the larger YSZ powder particles ($d_{50} \sim 45$ μm) which are coated or embedded within a thin layer of conductive material (nickel or LSM). The overall intent is for the zirconia particles to supply the electrode layers with a maximum of porosity along with a lower overall CTE value while the LSM or Ni constituents provide an interconnected network of electrically conductive material between the zirconia particles.

Significant levels of porosity are shown within both electrode microstructures. Both large pores between the zirconia particles and fine pores within the small sized particles are generated from the liquid deposition technique (See Fig. 4a and b). Melting of the smaller LIPD particles is observed and provides for an interconnected, electrically conductive network. Due to the limited melting of the larger YSZ particles, and the relatively thin deposition, only limited structural strength resides within these coatings.

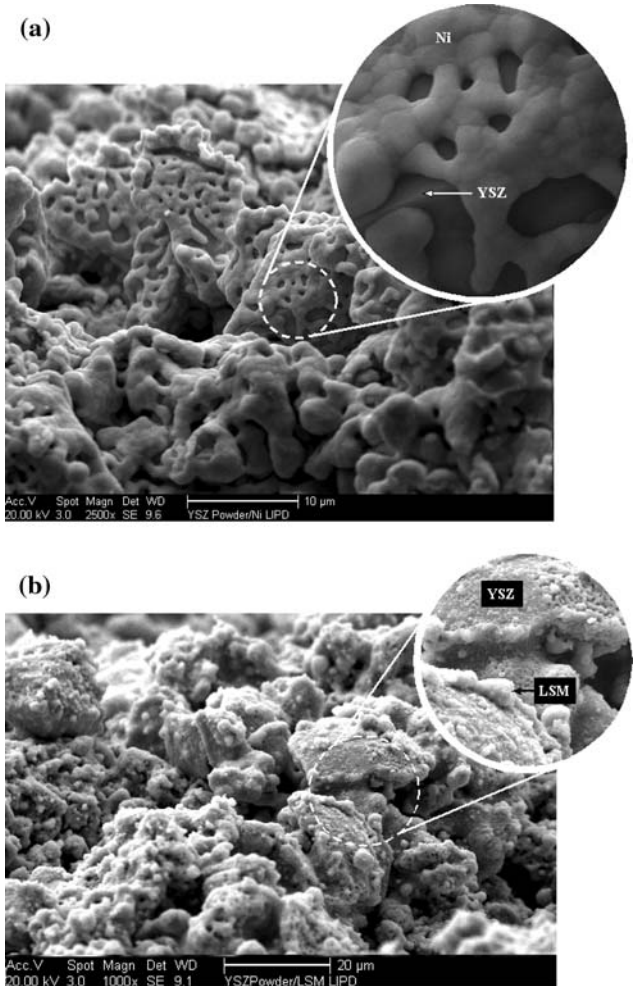

Fig. 4 SEM images of (**a**) LSM–YSZ anode layer and (**b**) Ni–YSZ cathode layer

It can clearly be seen (Fig. 4a) from the small tendrils of Ni formed on the flat surfaces of the zirconia particles that the nickel material does not readily wet the surfaces of the YSZ. Therefore, no significant chemical bonding is thought to exist between the metal and ceramic constituents, and the YSZ particles are seen to be embedded within an open network of conductive nickel. This structure allows significant gas transport and catalytic reactions to occur.

Unlike the nickel constituent in the cathode, only a limited amount of melting of the LSM oxide particles was expected. Small deposits of LSM were expected (and shown) to form on the YSZ ceramic oxide. This provides a more significant bond between the two oxide materials in the ceramic–ceramic composite microstructure (See Fig 4b). The fine porosity seen in the LSM deposit also provides a maximum of gas transport and triple phase boundary catalysis opportunities [13, 14].

It was initially found that electrode material examined directly after deposition was not electrically conductive indicating that the correct crystal structure had not been formed (i.e. the constituents were still in the form of nitrate salts). All deposits were heat treated to 800°C for 30 min to ensure decomposition of any remaining nitrate salts. The anode material required an oxygen-rich atmosphere to complete the formation of the desired *p*-type perovskite oxide crystal structure within the LSM constituent. However, to preclude the formation of nickel-oxides the nickel-bearing cathode coatings were heat treated in an inert gas environment (N_2).

X-ray diffraction (XRD) peaks (See Fig. 5) after heat treatment clearly show a $(La_xSr_y)MnO_3$ perovskite crystal structure forming in Fig. 5a as well as

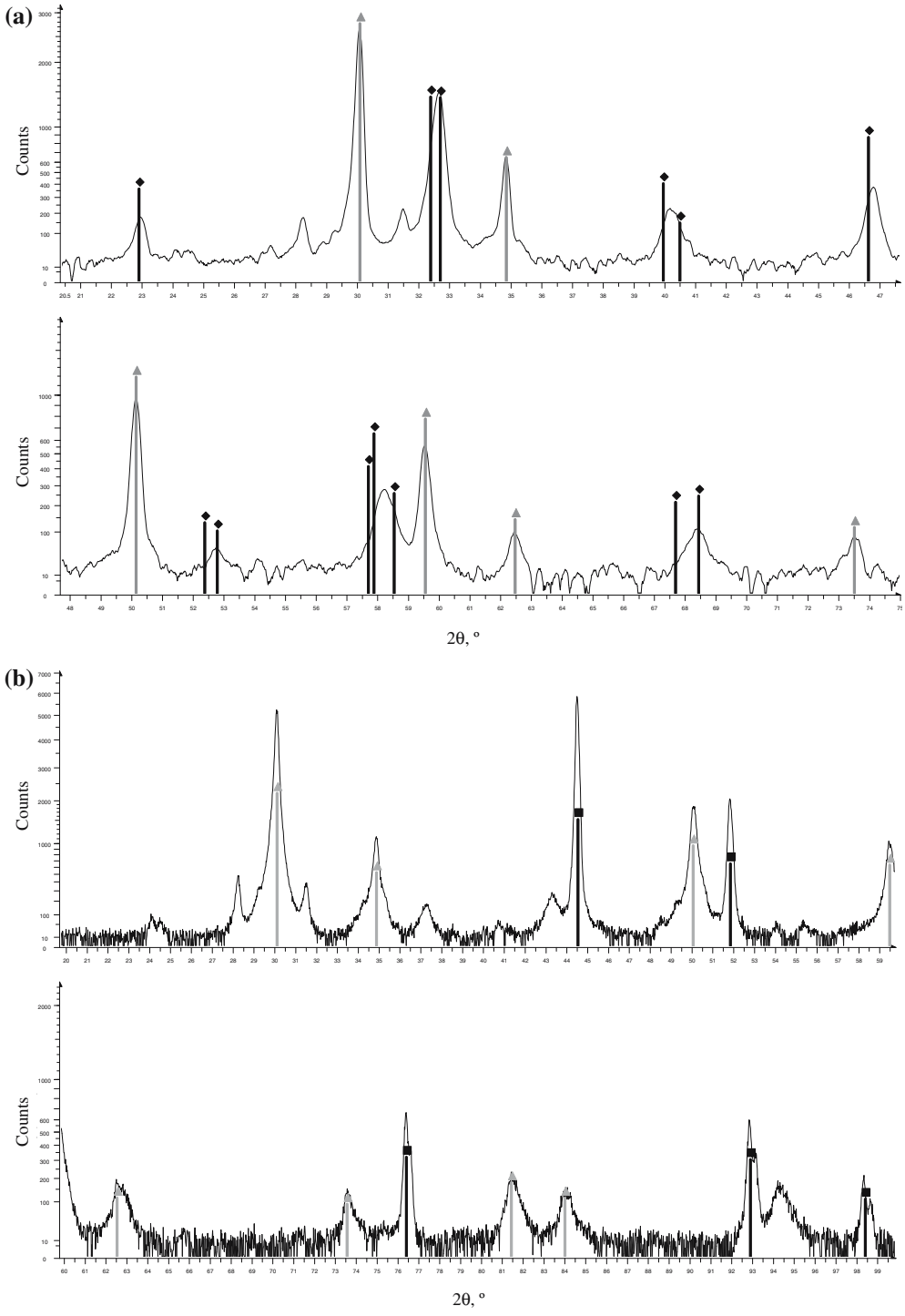

Fig. 5 X-Ray Diffraction (XRD) data for (**a**) LSM–YSZ anode and (**b**) Ni–YSZ coatings after deposition. YSZ ( ), LSM (◆), and Ni (■). (*Note:* reference peaks in 5(**a**) are for a LSM stoichiometry of $(LSM_{0.90}Sr_{1.0})MnO_3$)

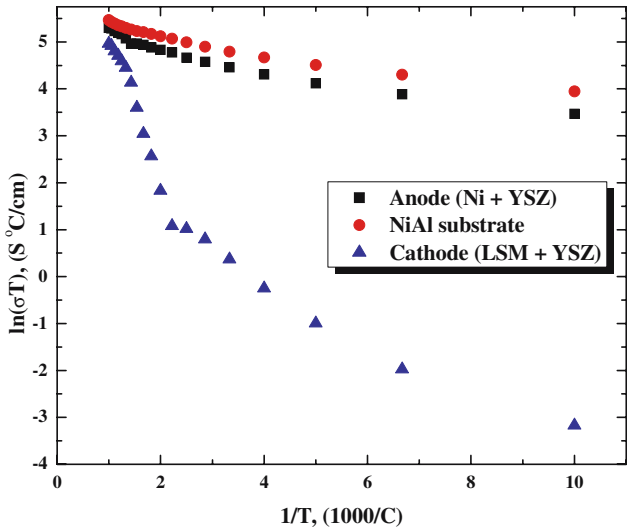

Fig. 6 Log conductivity versus reciprocal temperature for LSM–YSZ, Ni–YSZ, and NiAl substrate materials. Transition point for the LSM–YSZ deposition at ~500°C indicates reduced Sr dopant levels within the $(La_xSr_y)MnO_3$ perovskite structure

crystalline nickel forming in the microstructure in Fig. 5b. Small shifts in the LSM diffraction peaks indicate a small stoichiometry difference from the $(La_{0.9}Sr_{1.0})MnO_3$ XRD reference patterns used for identification. The most likely difference in stoichiometry is the Sr dopant levels inside the $LaMnO_3$ crystal structures, as discussed later. A significant pattern indicating large amounts of yttria stabilized zirconia present was found in both Fig. 5a and b (resulting from the addition of the large YSZ particles in both electrode microstructures).

Since the electrodes could be fabricated with microstructures exhibiting a desired level of porosity and the correct crystal structure, it remained to test the coatings for electrical conductivity at the anticipated operating temperatures (1000°C).

Electrical conductivity results

Electrical conductivity values for both electrode coatings (deposited on NiAl intermetallic substrates) were measured from room temperature to 1000°C and compared to the ''bare'' NiAl intermetallic substrate material with no deposited coatings (See Fig. 6). As expected, the electrical conductivity of the LSM–YSZ anode layer increases dramatically as the temperature approaches the operating temperature of 1000°C [15]. LSM forms a *p*-type perovskite oxide structure which conducts as a result of electron hole hopping between the +3 and +4 valence states of the Mn constituent [16, 17]. The hopping frequency increases exponentially as the temperature rises to the operating temperatures of the cell. The non-linear form of the Arrhenius plot indicates a low Sr dopant concentration within the LSM crystal structure [18]. Rather than the desired 10–20 mol% doping within the perovskite structures, these coatings most likely have a 5 mol% or less of Strontium within the $(La_xSr_y)MnO_3$ crystal structure. Further work will be necessary to optimize the dopant levels within the LSM anode layer using this deposition process.

The bare NiAl substrate and the NiAl + Ni–YSZ electrode showed similar conductivity values. The conductivity of the NiAl plus the Ni–YSZ electrode was slightly lower than for the bare NiAl substrate. While higher than the LSM–YSZ anode deposit, the conductivity of the cathode (Ni–YSZ) and substrate (NiAl) materials is still lower than predicted (based strictly upon a linear volume mixture).

Conductivity values for all test samples are lower than documented for pure, fully dense materials (Ni = 0.1 MS/cm and LSM = 80 S/cm) [15, 19]. These lower conductivity values are most likely due to the substantial levels of electrically insulating ceramic fillers in the conducting matrix (present in the NiAl substrate and both electrode layers). Based upon SEM visual observations it is estimated that the inert material and inherent porosity comprise nearly 75% of the volume in the electrode layers. This inert material reduces the electrical conductance density within the microstructure lowering the overall conductivity of the test samples. As discussed previously, the NiAl substrates have 32.5 vol% inert ceramic filler material as well as substantial porosity within the microstructure [9]. This will significantly reduce the electrical conductivity through the material.

Conclusions

Solid oxide electrolyzer electrode coatings for production of hydrogen were deposited upon NiAl intermetallic interconnect substrates. Utilizing liquid injection of nitrate solutions in conjunction with dry powder feedstock the plasma sprayed coatings displayed microstructures with a maximum of porosity. After heat treatment (in an oxygen-rich environment to form the *p*-type perovskite LSM crystal structure) the coatings were shown to be conductive in air up to temperatures of 1000°C. The lower conductivity of the electrode and interconnect materials resulted from a large volume of inert ceramic oxides within the microstructure to assist with CTE mismatch.

Acknowledgements This work was supported in part from funding from the DOE-NE Nuclear Hydrogen Initiative program.

References

1. Department of Energy, Energy Information Administration (2004) *International Energy Outlook*, DOE/EIA-0484(2004), April 2004
2. Department of Energy, Energy Information Administration (2005) *Annual Energy Outlook 2005*, DOE/EIA-0353(2005), February 2005
3. National Academy of Sciences, National Research Council (2004) *The hydrogen economy: opportunities, costs, barriers, and R&D needs*, February, 2004
4. Yildiz B, MS Kazimi (2003) MIT-NES-TR-001, September 2003
5. O'Brien JE, Stoots CM, Herring JS, Hartvigsen JJ, In: Shah RK, Kandlikar SG (eds) Proceedings of the ASME 3rd international conference on fuel cell science, engineering, and technology, May 23–25, 2005, Ypsilanti, MI, (ASME, 2005)
6. O'Brien JE, Herring JS, Stoots CM, Lessing PA (2005) In: Lemonnier H (ed) Proceedings of the 11th international topical meeting on nuclear reactor thermal-hydraulics NURETH-11, Popes Palace Conference Center, Avignon, France, October 2–6, 2005, (American Nuclear Society, 2005)
7. O'Brien JE, Stoots CM, Herring JS, Lessing PA (2004) In: Proceedings of the 2nd international conference on fuel cell science, engineering, and technology, June 14–16, 2004, Rochester, NY, p 219
8. Windes WE, Erickson AE, Lessing PA, Huestis G, Shaber E (2003) In: Singhal SC, Dokiya M (eds) Proceedings of solid oxide fuel cells VIII (SOFC-VIII), Paris France, April 27–May 2, 2003, Electrochemical Society, Inc., New Jersey, p 1109
9. Windes WE, Zuck LD, Shaber EL, Erickson AE, Lessing PA (2003) In: Singhal SC, Dokiya M (eds) Proceedings of solid oxide fuel cells VIII (SOFC-VIII), Paris France, April 27–May 2, 2003, Electrochemical Society, Inc., New Jersey, p 879
10. Liu H, Dandy DS (1995) Diamond Related Mater 4(10):1173
11. Charojrochkul S, Choy KL, Steele BCH (2004) J Eur Ceram Soc 24:2515
12. Windes WE, Lessing PA, Zuck LD (2002) In: Proceedings of 2002 fuel cell seminar, Palm Springs USA, November pp 18–21
13. Hart NT, Brandon NP, Day MJ, Shemilt JE (2001) J Mat Sci 36:1077
14. van Herle J, McEvoy AJ, Ravindranathan Thampi K (1996) Electrochemica Acta 41(9):1447
15. Plomp L, Booy A, van Roosmalen JAM, Cordfunke EHP (1990) Rev Sci Instrum 61(7):1949
16. Singhal SC (2000) MRS Bull 25(3):16
17. Haile SM (2003) Acta Materialia 51:5981
18. Kuo JH, Anderson HU, Sparlin DM (1990) J Solid State Chem 87:55
19. Gale WF, Totemeier TC (eds) (2004) Smithells metals reference book – 8th edn. Elsevier Inc., The Netherlands, pp 14–25